17th World Conference on Earthquake Engineering, 17WCEE
Sendai, Japan - September 13th to 18th 2020

Sliding-Rocking Combined Actions at Base Foundation Influencing Global and Local Deformations of Upper Wood Structure

T. Nagae[(1)], S. Uwadan[(2)], K. Takaya[(3)], C. Yenidogan[(4) (5)], S. Yamada[(6)], H. Kashiwa[(7)], K. Hayashi[(8)], T. Takahashi[(9)], T. Inoue[(10)]

[(1)] *Associate Professor, Nagoya University, nagae@nagoya-u.jp*
[(2)] *Graduate Student, Nagoya University*
[(3)] *Undergraduate Student, Nagoya University*
[(4)] *JSPS Fellow, Nagoya University, cem.yenidogan@gmail.com*
[(5)] *Assistant Professor, Bahçeşehir University, cem.yenidogan@eng.bau.edu.tr*
[(6)] *Associate, NIKKEN SEKKEI LTD, shohei.yamada@nikken.jp*
[(7)] *Senior Researcher, NILIM, kashiwa-h92ta@mlit.go.jp*
[(8)] *Assistant Professor, Toyohashi University of Technology, hayashi@ace.tut.ac.jp*
[(9)] *Senior Researcher, NIED, takehiro@bosai.go.jp*
[(10)] *Deputy Director, NIED, dinoue@bosai.go.jp*

Abstract

A three-story wood test building was prepared to assess the sliding-rocking combined action at the foundation as well as its influence to the response deformations of the upper wood structure. The test building adopted a generic construction method of the Japanese Grade-3 index building. A reinforced concrete foundation was constructed on a 1.5 m-high soil layer. Then, the upper wood structure was fully constructed anchored to the foundation. The entire test system was setup on the large shaking table facility at E-Defense, and a series of tests were conducted using Maximum-Considered-Earthquake motions. Regarding the foundation performance, the initial friction and cyclic friction strength capacities between the foundation and soil were quantitatively evaluated. Rocking at the foundation was assessed with theoretical uplifting capacities. Energy dissipation was calculated to the different deformation mechanism, and the distribution in the entire test system was shown.

Keywords: Shaking table test, Wood house, Soil-structure interaction, Functionality, Base isolation

1. Introduction

The 1995 Kobe earthquake and 2011 Tohoku earthquake caused catastrophic consequences to buildings and infrastructures. Solutions are the most important social issue in such earthquake-prone regions. Primary visions to enhance the resilience capacity of human communities have induced a shift of the relevant assessment methodology from approaches towards individual components to more comprehensive approaches towards entire building systems. This test program regarding full-scale wood dwellings produced real foundation-soil interactions. Figure 1 shows the test setup of a pair of three-story test buildings. B-building on the soil box adopted the special experimental function. [1] [2]

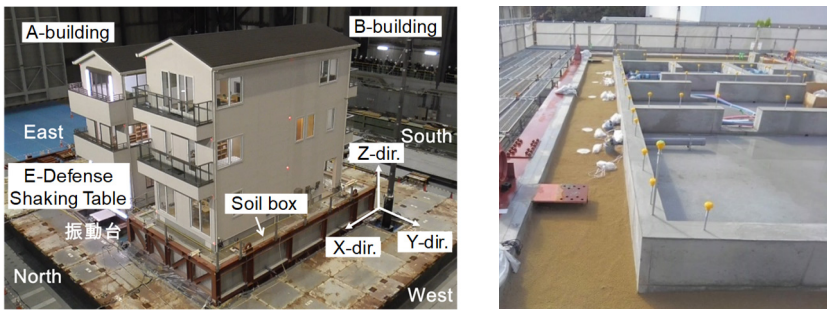

Fig. 1 Setup of the test building (B-building), and the foundation constructed on 1.5 m-high soil

2. Test System

The test system included the 1.5m-high soil in a rigid soil box of the size of 1.7 m (H) x 7.0 m (W) x 13.0 m (L). Silica sand was used for the soil layer. The soil base was divided into five layers with a height of 0.25 m. Each layer was inspected by the SWS test after compacting. Figure 2 shows the construction process. The locations of the SWS tests are also shown in the figure. Table 1 shows the results the SWS test. The inspected values reached three times the guideline requirement of 30 kN/m^2. The reinforced concrete foundation was designed assuming the equivalent ground condition. Then, the foundation was constructed according to a generic construction procedure, which started from a leveling concrete set and a broken stone foundation set. Figure 3 shows the plan and partial cross section of the foundation. Regarding the upper wood structure, a Shear-Wall structure known as the Two-by-Four construction was adopted. Figure 4 shows the plan of the first floor and framing elevation. The three-story building has a height of 9,879 mm and plan of 4,550 mm (X: Longitudinal direction) x 10,010 mm (Y: Span-direction).

Fig. 2 Construction of soil and locations of SWS test

Table 1 Soil evaluations by SWS test (allowable stress values for sustained loading)

SWS test for soil	(1)	(2)	(3)	(4)	(5)	Average
(kN/m^2)	85.2	89.4	82.8	81.0	86.4	85.0

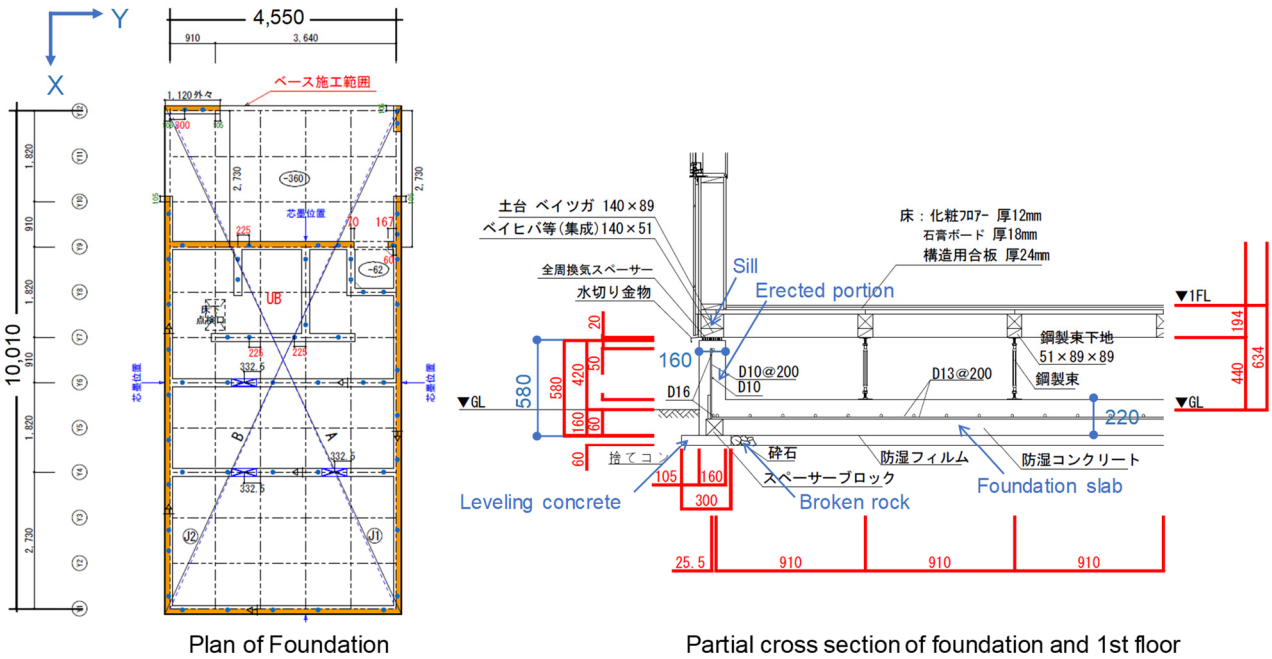

Fig. 3 Plan and cross section of reinforced concrete foundation

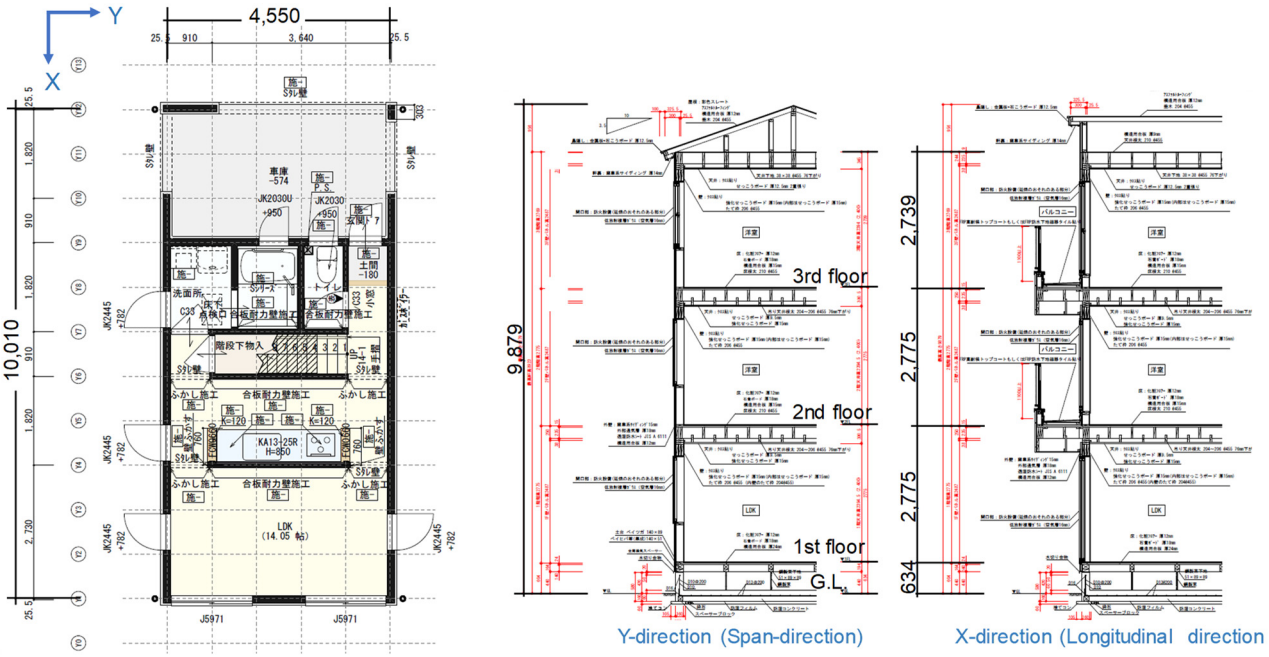

Fig. 4 Plan of the first floor and framing elevation

The design of the Grade-3 index building was applied. The stress margin to the requirement was minimized. That is, the design stress level to the design base shear coefficient of 0.3 was close to the allowable stress level. The total weight was 790.9 kN. This consisted of the roof level (79.9 kN), third floor level (146.9 kN), second floor level (149.7 kN), first floor level (71.0 kN), and foundation (343.4 kN). Table 2 shows the seismic force used in the design.

Table 3 shows the physical boundary conditions of the test systems in each sequential test of Phase 1, Phase 2 and Phase 3. In the first Phase 1, the foundation was set on soil. In the second Phase 2, twenty cast iron plates were inserted between the foundation slab and soil to change the friction resistance. Note that cast iron is known as a steady lubricant. [3] Figure 5 shows the locations of the cast iron plates in the foundation plan. The installation procedure is also shown in the figure; the soil was excavated from the exterior parts of the foundation, and after installing the cast iron plates, the same original soil was returned and compacted. The remained parts of leveling concrete were removed in this process. In the third Phase 3, the foundation slab was firmly fixed to the rigid soil box by stiff steel beams and high-tension bolts.

Figure 6 shows the setup process of the test system to the E-Defense table. The sequential process of carrying, lifting and placing on the E-Defense table was carefully and slowly proceeded. Conditions of the foundation on soil were stable in the rigid soil box. After placing the test system on the table, the bottom flange of the soil box was firmly fixed to the table with a number of prestressing steel bars.

Table 2 Seismic force used in the allowable stress design

	Total weight Σwi **(kN)**	Ai	**Shear force coefficient** Ci	**Seismic force** eQi **(kN)**
3rd story	79.91	1.60	0.480	38.32
2nd story	226.83	1.21	0.363	82.31
1st story	376.50	1.00	0.300	112.95

Table 3 Testing program and boundary conditions of foundation

Phase / Test date	Input motion	Condition of foundation
Phase 1 January 31, 2019 February 1, 2019	(1) JMA-Kobe 25% (2) JMA-Kobe 50% (3) JR-Takatori 25% (4) JR-Takatori 50% (5) JMA-Kobe 100% (6) JR-Takatori 100%	Foundation slab set on soil
Phase 2 February 7, 2019	(7) JMA-Kobe 25% (8) JMA-Kobe 50% (9) JMA-Kobe 100% (10) JR-Takatori 100%	Cast iron plates inserted between foundation slab and soil
Phase 3 February 12, 2019	(11) JMA-Kobe 100%	Firmly fixed foundation

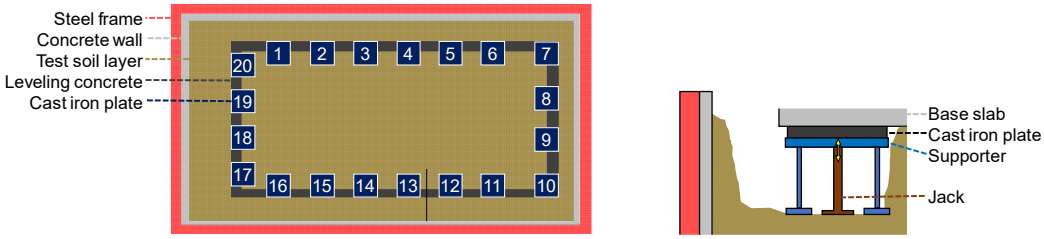

Fig. 5 Locations of twenty cast-iron plates in the foundation plan and the installation procedure

Fig. 6 Setup process of the test system to the E-Defense table

3. Test Results

The acceleration spectra were evaluated by sensors placed on the foundation slab and shaking table. Figure 7 shows the comparisons of acceleration spectra evaluated in Phase 1. The spectra of the foundation slab and the shaking table were identical in the X and Y-directions in JMA-Kobe 50%. The results of JMA-Kobe 100% were different from JMA-Kobe 50%. The spectrum amplitude of the foundation slab was smaller than that of the shaking table in the period range of 0.3 sec -1.0 sec in each direction. The same trends were observed in

JR-Takatori 100%. The spectrum amplitudes of foundation were lager than that of that shaking table at the period range of 0 – 0.8 sec in the Z-direction. The horizontal acceleration spectrum was influenced by sliding of the foundation, and the vertical acceleration spectrum was influenced by rocking of the foundation, as stated below.

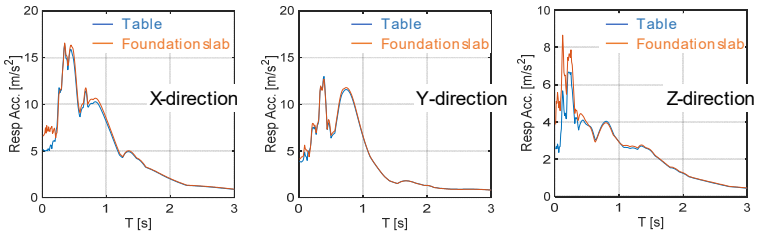

(1) JMA-Kobe 50%

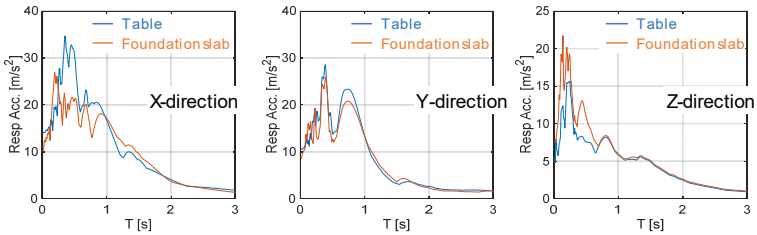

(2) JMA-Kobe 100%

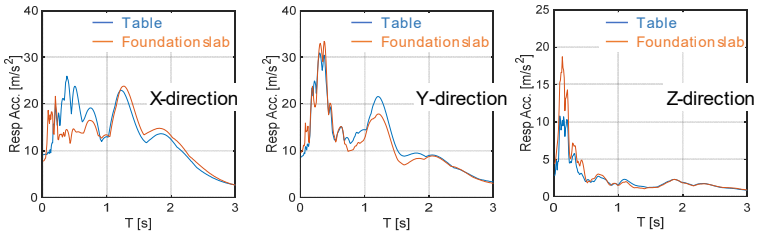

(3) JR-Takatori 100%

Fig. 7 Acceleration spectra evaluated by sensors placed on the foundation slab and shaking table

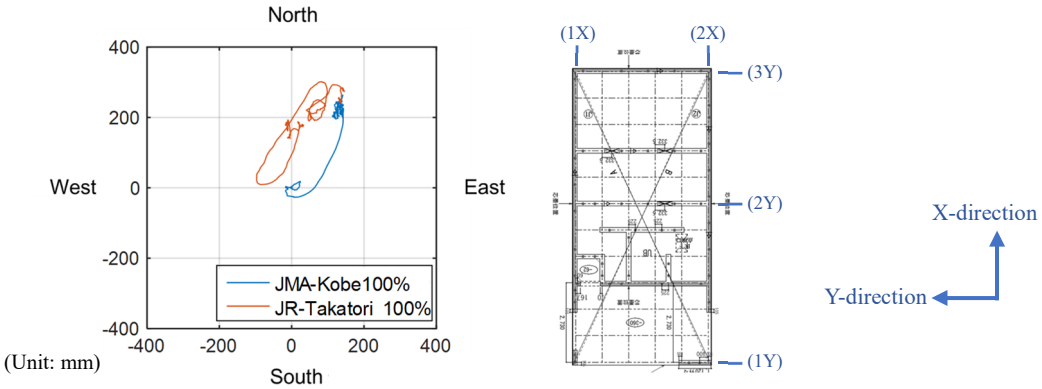

Fig. 8 Sliding displacement orbit of foundation during JMA-Kobe 100% and JR-Taktori 100%

Regarding the tests of Phase 1, Figure 8 depicts the orbits of two-directional sliding displacement at the foundation. Figure 9 shows the time histories of the sliding displacement in the sequential tests. The maximum lateral sliding displacement reached 240 mm in the X-direction and 100 mm in the Y-direction during JMA-Kobe 100%. The maximum lateral sliding displacement reached 300 mm in the X-direction during JR-Takatori 100%. The foundation moved around on the soil without touching the soil box.

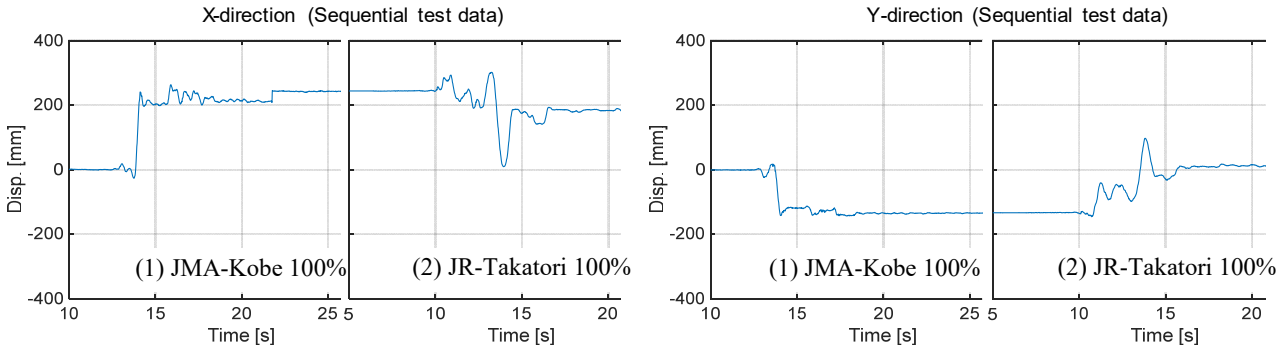

Fig. 9 Sliding displacement time history in the sequential tests of Phase 1

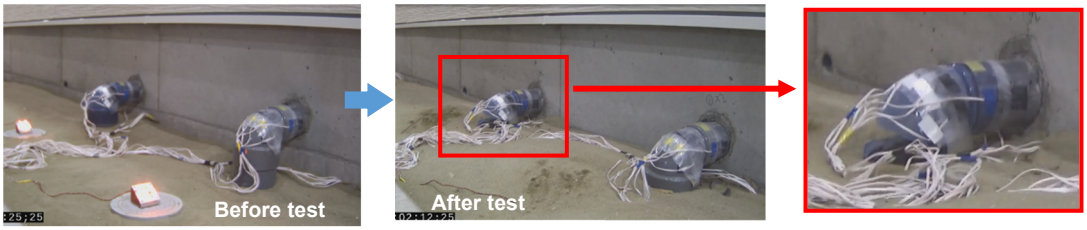

(1) VP drain pipe line system

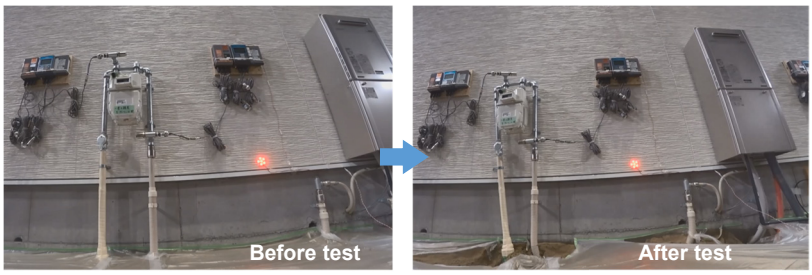

(2) Polyethylene gas pipe system

Fig. 10 Embedded pipelines dragged by sliding foundation when subjected to JMA-Kobe 100%

Figure 10 shows the embedded pipelines were dragged by the sliding foundation when subjected to JMA-Kobe 100% in Phase 1. Brittle VP drainpipes were fractured resulting in a significant loss of the functionality. On the other hand, polyethylene gas pipe system showed high deformability, as shown in Fig. 10 (2), but maintained the inside gas pressures even after the test of JR-Takatori 100%.

3.1 Hysteretic Behaviors of Foundation and Upper Structure / Phase 1

Figure 11 shows the hysteretic behaviors of the foundation and upper structure observed in the tests of Phase 1. Figure 11 (1) shows the relationship of the shear force coefficient and sliding displacement of the foundation, and Fig.11 (2) shows the relationship of the story shear force coefficient and story drift angle at the first story. The figure legend, D1/X1 stands for the record of X1 axis shown in Fig. 8. The axes of X2, Y1, Y2 and Y3 are also shown in Fig. 8. In JMA-Kobe 50%, the maximum sliding displacement of the foundation was only 3.5 mm. The maximum shear force coefficient of the foundation was 0.63 in the X-direction and 0.45 in the Y-direction. The maximum story drift angle was 0.003 rad in the X-direction and 0.007 rad in the Y-direction. In JMA-Kobe 100%, the maximum sliding displacement reached 240 mm in the X-direction, while the maximum shear force coefficient of the foundation was 0.91 in the X-direction. The maximum story drift

angle was 0.008 rad in the X-direction and 0.015 rad in the Y-direction. In JR-Takatori 100%, the maximum shear force coefficient of the foundation was smaller than that of JMA-Kobe 100%, and was 0.68 in the X-direction. The maximum story drift angles were close values of JMA-Kobe 100%, and 0.008 rad in the X-direction and 0.015 rad in the Y-direction.

Regarding the response of the foundation, the highest value of shear force coefficient of 0.91 was shown at the start moment of the first sliding in JMA-Kobe 100%. The shear force coefficient decreased and kept the values at around 0.6 during JR-Takatori 100%. This indicates that shear failure occurred in the soil beneath the foundation with significant first sliding and the condition of the soil changed to a relatively stable condition. Regarding the responses of the upper structure, the maximum story shear force coefficient was 0.8 in JMA-Kobe 50% and 1.2 in JMA-Kobe 100%. The stiffness remained even in JMA-Kobe 100%. That is, the shear force response of the first story became 1.5 times when the input motion was increased by two times. This indicates that the sliding of the foundation provided the upper limit of the shear force in the upper structure.

3.2 Hysteretic Behaviors of Foundation and Upper Structure / Phase 2

Figure 12 shows the hysteretic behaviors of the foundation and upper structure in Phase 2. Figure12 (1) shows the relationship of the shear force coefficient and sliding displacement beneath the foundation, and Fig.12 (2) shows the relationship of the story shear force coefficient and story drift angle at the first story. During JMA-Kobe 50%, the foundation started sliding, and the maximum sliding displacement of the foundation reached 100 mm. The maximum shear force coefficient of foundation was 0.48 in the X-direction

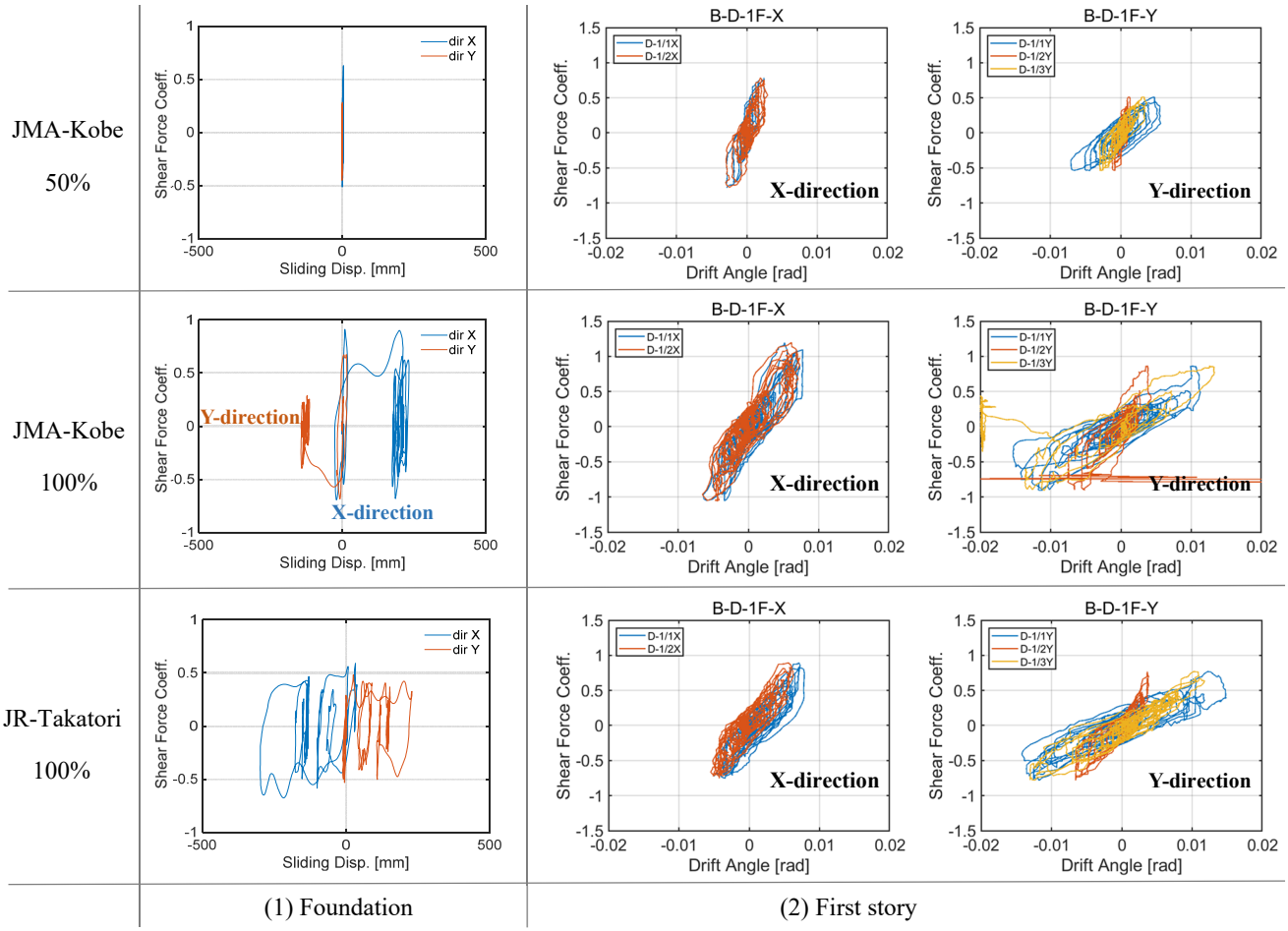

Fig. 11 Foundation- soil system: (1) Shear force coefficient and sliding displacement at the foundation, (2) Story shear force coefficient and story drift angle at the first story

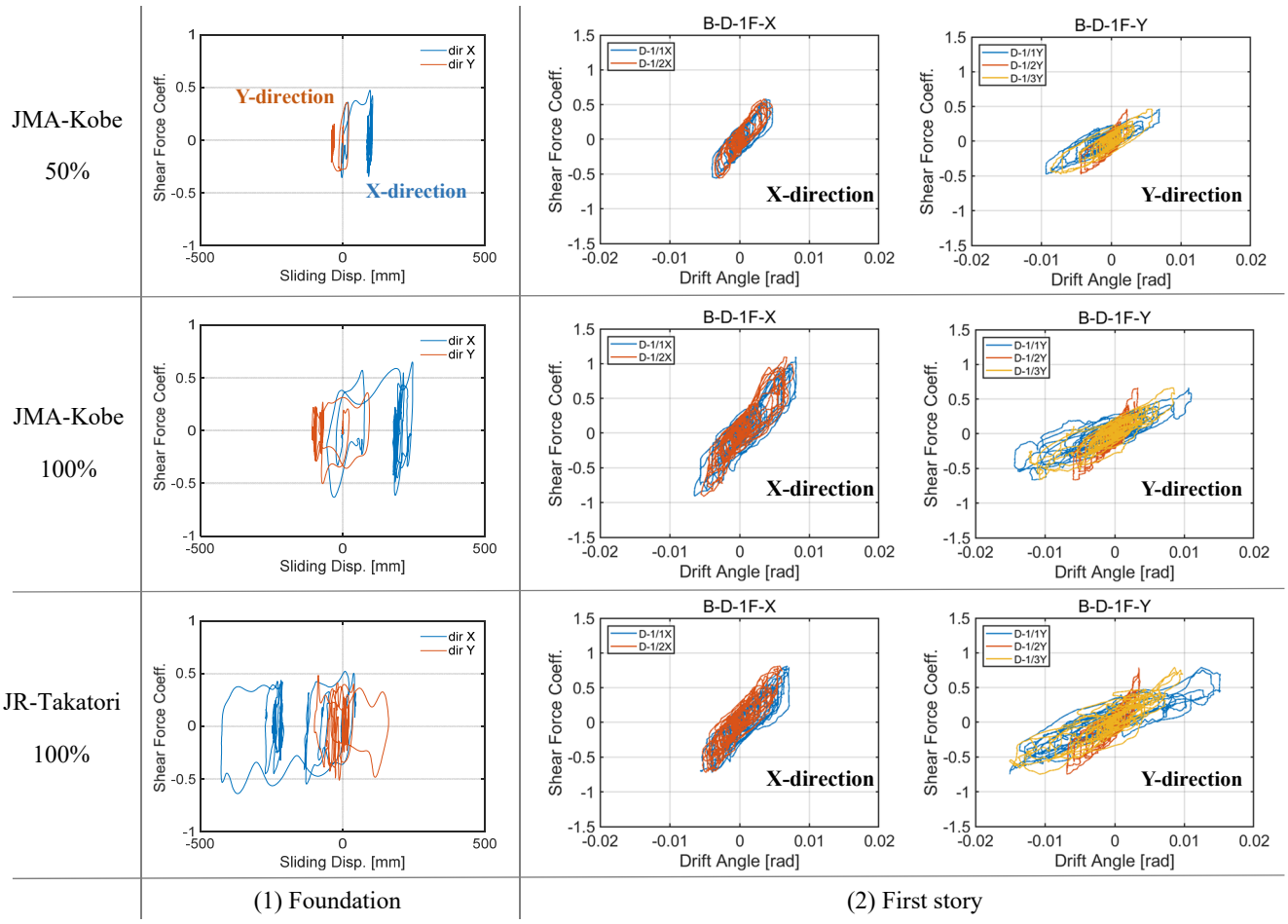

Fig. 12 Foundation -cast iron plate-soil system: (1) Shear force coefficient and sliding displacement at the foundation, (2) Story shear force coefficient and story drift angle at the first story

and 0.36 in the Y-direction. The maximum story drift angle was 0.003 rad in the X-direction and 0.008 rad in the Y-direction. When subjected to JMA-Kobe 100%, the maximum shear force coefficient of foundation was 0.65 in the X-direction. The maximum sliding displacement exceeded 300 mm in the X-direction. The maximum story drift angle was 0.008 rad in the X-direction and 0.014 rad in the Y-direction. During JR-Takatori 100%, the maximum shear force coefficient of the foundation was smaller than that of JMA-Kobe 100%, and was 0.64 in the X-direction. The maximum sliding displacement exceeded 400 mm. The maximum story drift angles were 0.007 rad in the X-direction and 0.015 rad in the Y-direction. Regarding the response of the foundation, the shear force coefficient gradually increased from 0.3 to 0.6 as the sliding displacement increased. The presence of cast iron plates was effective in JMA-Kobe 50%. Regarding the responses of the upper structure, the maximum story shear force coefficient became lower in Phase 2 than in Phase 1 when subjected to JMA-Kobe 50%.

3.3 Overturning Moment and Rocking Rotation of Foundation

Figure 13 shows the relationship between the overturning moment and rocking rotation angle at the foundation slab when the test building was subjected to JMA-Kobe 50% and JMA-Kobe 100%. The two horizontal dotted lines show the decompression moment and ultimate moment reflecting the total weight (See the illustration shown in the upper part of Fig.13). During JMA-Kobe 50%, the overturning moment exceeded the decompression moment in both the X and Y-directions. The relationship maintained the first gradient, and the rotation angle slightly exceeded 0.002 rad in the Y-direction. During JMA-Kobe 100%, the relationship

showed different shapes in the X and Y-directions; with the overturning moment slightly exceeding the ultimate moment, the rocking rotation reached 0.015 rad. The ceiling of the overturning moment due to uplift of the foundation slab provided the upper limit of overturning moment to the wall base level.

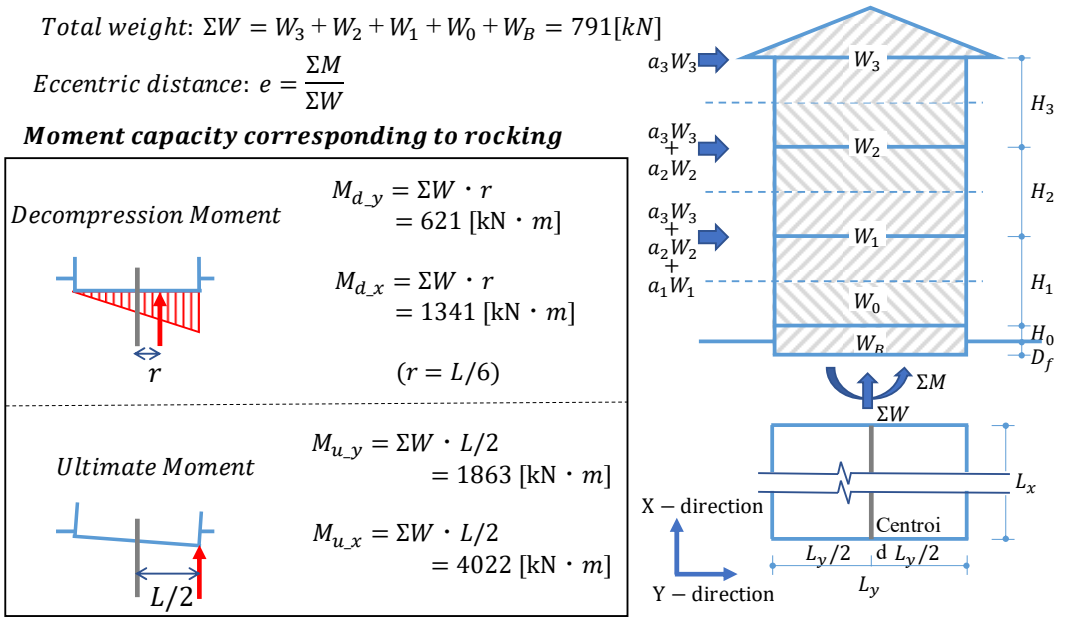

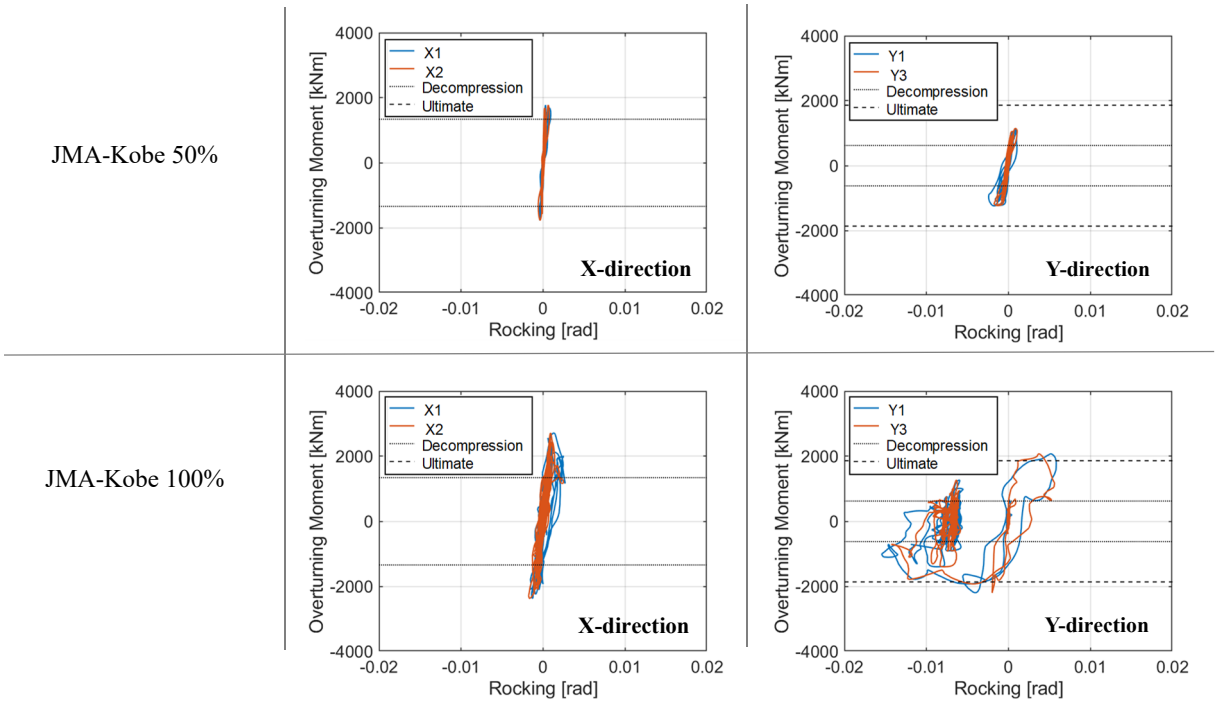

Fig. 13 Overturning moment and rocking rotation angle at foundation (Phase 1)

4. Energy Dissipation in Comparison to the Fixed Foundation Case

In the condition of the fixed foundation, the shaking table input was fully applied to the foundation in Phase 3. As a result, significant fractures of the wall bases occurred between the sills and shear wall panels.[2] Figure 14 shows the relationships between the base shear force coefficient and drift angle when subjected to JMA-Kobe 100% in Phase 3. The maximum drift angle reached 0.08 rad in the X-direction, and exceeded 0.1 rad in the Y-direction. The shear force decreased to less than 20 % of the maximum shear force. The relationships of the Phase 1 tests are added in the figure. The sliding and uplifting of the foundation provided the upper limit of seismic force to the upper structure in Phase 1. Therefore, the upper structure avoided the ultimate failure, and the maximum drift angles were limited to 0.018 rad.

Figure 15 shows the total energy dissipation including the results of other test cases. [1][2] The entire test program was planned with another test building adopting the Post-and-Beam structure (A-building). In the first stage, Phase 1, A-building accommodated a generic base isolation system, and in the following Phase 2, its foundation was firmly fixed. In each test case shown in the lower part of Fig.15, the total energy dissipation

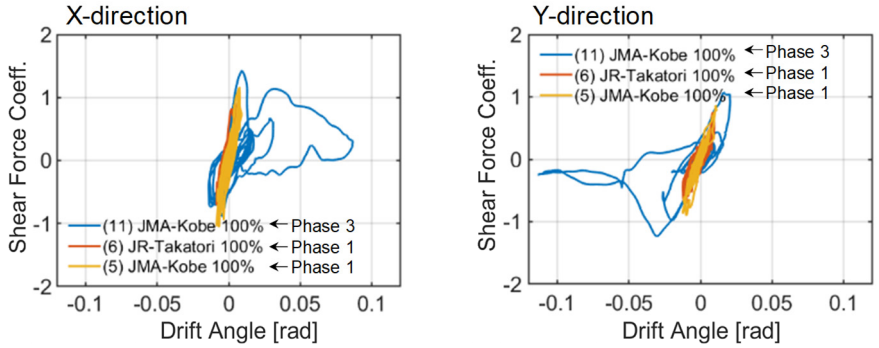

Fig. 14 Comparisons of responses of upper structure in Phase 3 and in Phase1

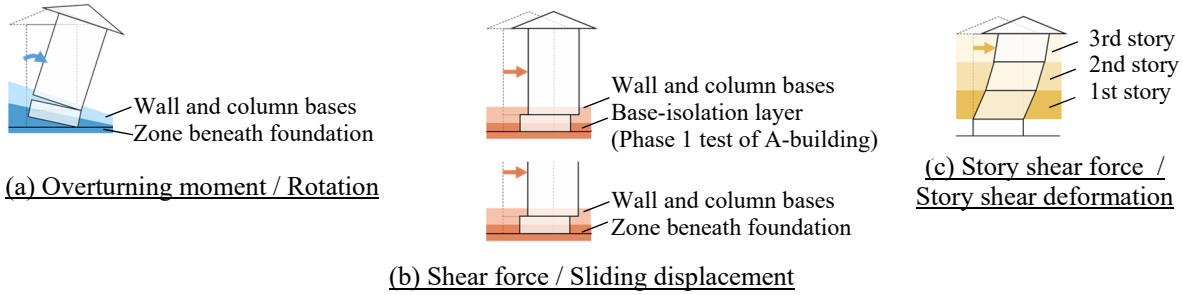

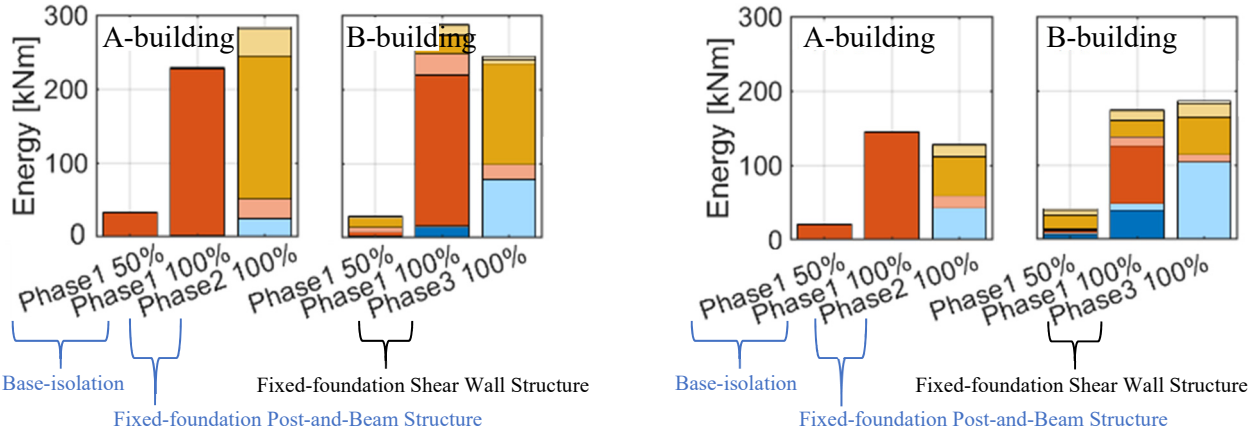

Fig. 15 Distribution of energy dissipation in the entire structural system (JMA-Kobe 50% and 100%)

was calculated in reference to the hysteretic behavior of each local deformation mode and the corresponding seismic forces depicted in the upper part of Fig.15. The evaluations of total energy dissipation are equivalent in JMA-Kobe 50% and JMA-Kobe 100%, respectively. Regarding JMA-Kobe 100 %, the energy dissipation of B-building mostly occurred at the foundation in Phase 1, but mostly in the upper structure in Phase 3. The total values of energy dissipation are equivalent. The same trends are also derived from the other test cases of A-building, which adopted the condition of the first base isolation system and the second fixed foundation. That is, when the upper structure has a strength capacity sufficient to cause the foundation to slide or rock, the total system exhibits a similar energy dissipation mechanism to the base-isolation system.

5. Conclusions

A three-story wood test building was prepared to assess the sliding-rocking combined action at foundation as well as its influence to the response deformations of the upper wood structure. The test building adopted a generic construction method of the Japanese Grade-3 index building. A reinforced concrete flat foundation was constructed on a 1.5 m-high soil layer. Then, the upper structure was constructed to represent an entire building structure. Regarding the foundation sliding, shear strength and cyclic friction strength were quantitatively evaluated. Uplifting due to the foundation rocking was assessed with the theoretical evaluations. The upper structure avoided critical failure due to wall base fractures because such inelastic behavior at the foundation provided the upper limit of seismic force to the upper structure. Energy dissipation distributions including the other synchronizing tests indicated that the energy input of ground motion was mostly shared by the foundation exhibiting the inelastic deformation. Such energy dissipating mechanism was similar to a generic base isolation system. The effect of damage mitigation was significant in the Maximum-Considered Earthquake level.

Appendix 1: Overturning Moment and Resisting Moment

Total energy dissipation due to rocking of the foundation can be calculated in reference to the hysteretic loops of the over-turning moment and rocking rotation in each X-Y direction. On the other hand, in order to calculate the energy dissipation due to compressive force and deformation in soil, the compressive zone was defined assuming the total compressive force is equal to the total weight (Appendix-fig. 1). The vertical displacement data of the foundation was used to define the compressive zone. Appendix-fig. 2 shows the examples of calculated vertical displacement distribution of the foundation slab. Appendix-fig. 3 shows the assumed compressive hysteresis of soil. The energy dissipation values assessed by two methods indicate that the total energy dissipation due to rocking of the foundation is equivalent to the energy dissipation of compressed soil.

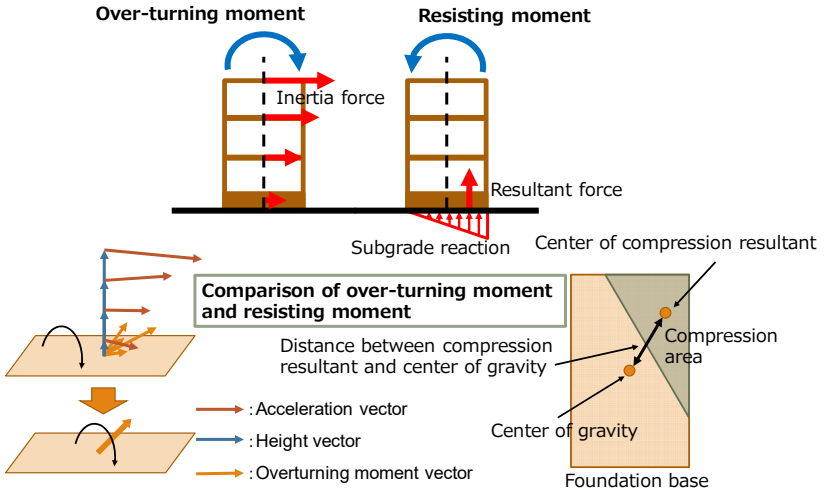

Appendix-fig. 1 Overturning moment of the upper structure and resisting moment of the foundation

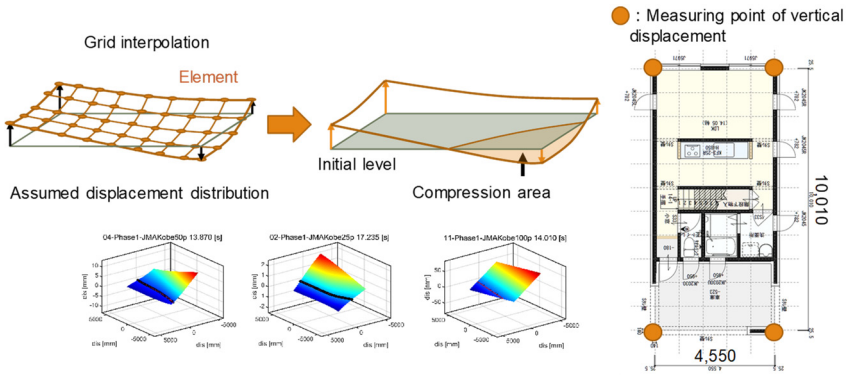

Appendix-fig.2 Compressive displacement distribution converted the vertical displacement records

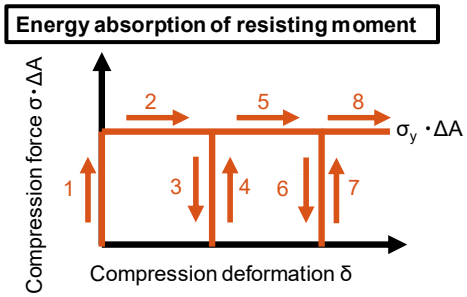

Appendix- fig 3 Compressive hysteresis assumption in each grid of compressive zone of soil

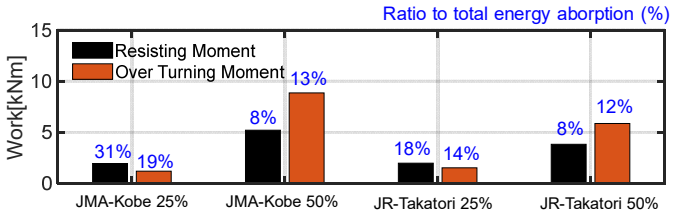

Appendix- Fig. 4 Comparison of calculated energy dissipation

5. Acknowledgements

This work is supported by the Tokyo Metropolitan Resilience Project of the National Research Institute for Earth Science and Disaster Resilience (NIED). Collaboration on earthquake engineering research using E-Defense and NHERI facilities is proceeding continuously. Construction of the test buildings was managed by ICHIJO Co., Ltd. Test-relevant affairs were administrated by the Graduate School of Environmental Studies, Nagoya University and E-Defense, NIED.

6. References

[1] T. Nagae, S. Uwadan, C. Yenidogan, S. Yamada, H. Kashiwa, K. Hayashi, T. Takahashi, T. Inoue (2020): The 2019 full-scale shake table test program of wood dwellings. *17th World Conference on Earthquake Engineering, 17WCEE*, Paper No. C002274.

[2] T. Takahashi, T. Nagae, S. Uwadan, C. Yenidogan, S. Yamada, H. Kashiwa, K. Hayashi, T. Inoue (2020): Stiffness, ultimate strength capacity and cyclic loading deterioration characteristics of two different wood-structure dwellings following the current Japanese practice. *17th World Conference on Earthquake Engineering, 17WCEE*, Paper No. C002285.

[3] R. Enokida, T. Nagae, M. Ikenaga, M. Inami, M. Nakashima, (2013): Application of graphite lubrication for column base in free standing steel structure, J. Struct. Constr. Eng., AIJ, Vol. 78 No. 685, 435-444 (in Japanese)

